Deep-Sea Research Part II 168 (2019) 104645

Contents lists available at ScienceDirect

Deep-Sea Research Part II

journal homepage: www.elsevier.com/locate/dsr2

Freshwater export pathways from the Bay of Bengal

Verena Hormann[a,*], Luca R. Centurioni[a], Arnold L. Gordon[b]

[a] Scripps Institution of Oceanography, UC San Diego, La Jolla, CA, USA
[b] Lamont-Doherty Earth Observatory, Columbia University, Palisades, NY, USA

ARTICLE INFO

Keywords:
Advection
Air-sea interaction
Drifters
Freshwater
Mesoscale features
Monsoons
Salinity
Seasonal variations
Surface currents
Tropical oceanography
Upper ocean
Water exchange

ABSTRACT

Observations from surface drifters and Argo floats elucidate details of two upper-ocean pathways through which freshwater from the Bay of Bengal (BoB) is advected into the tropical Indian Ocean and Arabian Sea (AS). The western route is located along the east coast of India and feeds into the westward Northeast Monsoon Current (NMC) south of Sri Lanka during the winter monsoon, whereas the eastern path is located along the western margin of Sumatra reaching at times as far south as the Indonesian Throughflow plume near 10°S. While the former pathway is highly seasonal and affected by mesoscale variability, the latter is a year-round feature and may be dominant from an annual perspective. The observations do not support the notion of a continuous current system comprised of the NMC and the West India Coastal Current around the Laccadive High in boreal winter that can directly export surface freshwater from the BoB to the AS. Further, the observations indicate an occasional leakage of low-salinity water by a westward coastal current between the eastward Southwest Monsoon Current (SMC) and Sri Lanka in boreal summer that may be caused by equatorial wave processes. The SMC, which exhibits considerable Ekman contributions in contrast to its geostrophically-balanced NMC counterpart in boreal winter, facilitates the transport of saltier AS water into the BoB, with subsequent spreading into the upper thermocline of the BoB setting up an estuary-like circulation pattern.

1. Introduction

The two northern embayments of the Indian Ocean, the Bay of Bengal (BoB) and Arabian Sea (AS), show remarkably contrasting sea surface salinity (SSS) values and distributions despite their comparable latitudinal range, with a SSS difference of more than 3 psu (Fig. 1). During the South Asian monsoon, the BoB receives large amounts of freshwater from rainfall and river runoff. Conversely, the AS is characterized by excess evaporation (e.g. Rao and Sivakumar, 2003; Sengupta et al., 2006). While the freshwater input into the BoB (i.e. precipitation and river runoff minus evaporation) is +0.13 Sv (Sv = $10^6\,m^3s^{-1}$), there is a freshwater loss of −0.11 Sv in the AS (e.g. Sengupta et al., 2006; Gordon et al., 2016). One of the currently accepted hypotheses is that apart from localized vertical mixing, which is responsible for freshwater fluxes at the base of the thermocline, the quasi-steady SSS state of the BoB and AS is dominated by the interchange of their waters; that is, the upper-ocean circulation exports low-salinity surface water from the BoB into the AS, compensated by saltier AS water advected into the upper thermocline of the BoB. The latter requires upward mixing of subsurface waters into the surface layer (e.g. Vinayachandran et al., 2013) or isopycnal spreading of saline water toward the northern BoB (e.g. Rao and Sivakumar, 2003).

Forced by reversing monsoon winds and associated reversals and seasonality of the near-surface currents (Fig. 1; e.g. Schott and McCreary, 2001; Schott et al., 2009), the interbasin exchange processes are also highly seasonal and modulated by intraseasonal oscillations (e.g. Vinayachandran et al., 2013; Wijesekera et al., 2015) as well as by interannual and longer timescale cycles (e.g. Rao and Sivakumar, 2003; Jensen, 2007; Pant et al., 2015; Akhil et al., 2016). Both numerical models (e.g. Jensen, 2007) and observations (e.g. Pant et al., 2015) indicate that the average clockwise circulation in the tropical Indian Ocean is intensified during El Niño as well as positive Indian Ocean Dipole years and weakened during La Niña years, with implications for the upper-ocean water mass exchanges between the BoB and AS. While local freshwater fluxes dominate upper-ocean mixed-layer salinity during the summer southwest monsoon, horizontal dispersion and advection become of prime importance during the winter northeast monsoon (e.g. Rao and Sivakumar, 2003; Pant et al., 2015). Although the basin-wide circulation and associated salinity advection are largely wind-driven, the monsoonal forcing also generates energetic meso- and submesoscale features that can obscure the regional upper-ocean patterns (e.g. Gordon et al., 2016). The circulation in the BoB is further complicated by Kelvin and Rossby wave radiation from the eastern boundary of the tropical Indian Ocean (e.g. Rao et al., 2010).

* Corresponding author.
E-mail address: vhormann@ucsd.edu (V. Hormann).

https://doi.org/10.1016/j.dsr2.2019.104645
Received 14 January 2019; Received in revised form 4 September 2019; Accepted 5 September 2019
Available online 06 September 2019
0967-0645/ © 2019 The Authors. Published by Elsevier Ltd. This is an open access article under the CC BY license (http://creativecommons.org/licenses/by/4.0/).

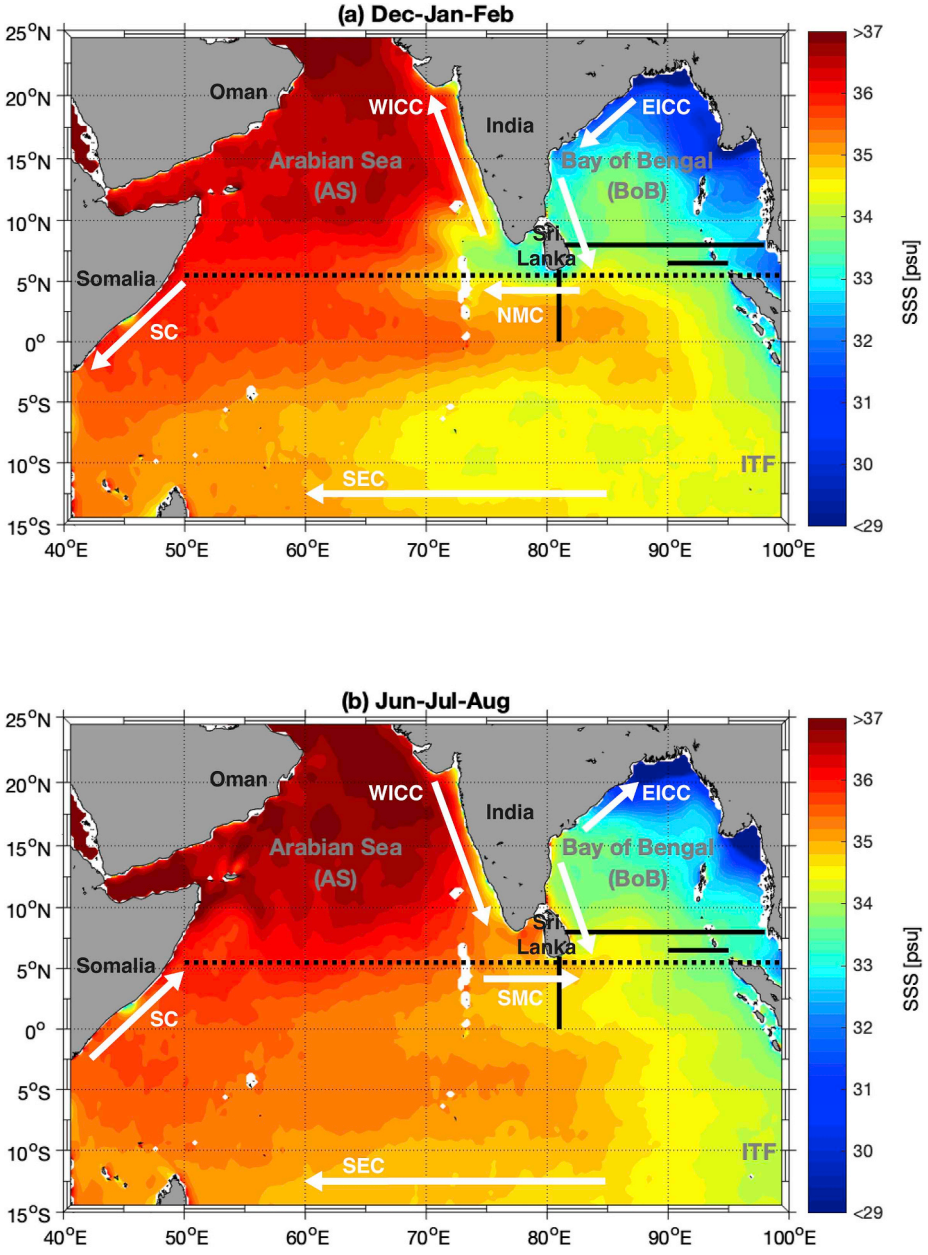

Fig. 1. Maps of 4-year mean SMAP SSS (color), with superimposed major surface currents (white arrows; see text for details): (a) December-January-February, and (b) June-July-August. Black lines mark transects along 81°E, 8°N, and 6.5°N (solid) as well as 5.5°N (dotted). (For interpretation of the references to color in this figure legend, the reader is referred to the Web version of this article.)

There are two main surface pathways through which freshwater can be removed from the BoB. The first one is located along the east coast of India and around Sri Lanka and is associated with the southward East India Coastal Current (EICC) that occurs during late boreal fall and early boreal winter and flows into the southeast AS forming then the westward Northeast Monsoon Current (NMC; e.g. Shetye et al., 1996; Wijesekera et al., 2015). The second one is located along the eastern margin of the tropical Indian Ocean. Ocean circulation models (e.g. Jensen, 2001 and 2003; Benshila et al., 2014; Behara and Vinayachandran, 2016) and observational studies (e.g. Sengupta et al., 2006; Pant et al., 2015) have shown that low-salinity BoB water is at times exported southward in the eastern BoB before crossing the equator and turning westward within the South Equatorial Current (SEC) upon encountering the Indonesian Throughflow (ITF). However, recent model studies disagree on the primary source of this freshwater export (i.e. rainfall or river runoff) which is most pronounced in the second half of the year (e.g. Benshila et al., 2014; Behara and Vinayachandran, 2016). While the major inflow of saltier water into the BoB occurs within the Southwest Monsoon Current (SMC) during boreal summer (e.g. Schott and McCreary, 2001; Jensen, 2001and 2003), subsurface northward flow carrying high-salinity water into the BoB has also recently been observed during the winter northeast monsoon (e.g. Wijesekera et al., 2015).

Using near-surface current observations from Lagrangian Surface Velocity Program (SVP) drifters drogued at 15-m depth and subsurface Argo floats, we examine the dominant freshwater export pathways from the northern BoB into the tropical Indian Ocean and AS as well as the relative roles of the Ekman and geostrophic velocity components (e.g. Hastenrath and Greischar, 1991) and the potential importance of mesoscale features in critical exchange regions (e.g. Durand et al., 2009).

2. Data and methods

2.1. Surface drifters

In their basic configuration, the SVP drifters provide observations of 15-m currents (i.e. center depth of the drogue) and sea surface temperature but they can also be equipped with additional sensors to measure surface salinity, sea-level atmospheric pressure as well as sea-level wind (e.g. Centurioni, 2018). For this study, historical near-surface current observations from satellite-tracked Lagrangian SVP drifters from the Global Drifter Program (GDP) archive are used (Niiler, 2001; Maximenko et al., 2013; Centurioni, 2018) which start in the Indian Ocean in 1985 and include recent observations from drifters deployed under the Office of Naval Research (ONR) Departmental Research Initiatives ASIRI (Air-Sea Interactions in the Northern Indian Ocean – Regional Initiative; Wijesekera et al., 2016) and NASCar (Northern Arabian Sea Circulation – autonomous research; Centurioni et al., 2017). These ONR-sponsored programs were critical to enhance the historically sparse data coverage in the tropical Indian Ocean by way of targeted deployments in the critical exchange region around Sri Lanka (Wijesekera et al., 2015; Lee et al., 2016), in the northern BoB (Hormann et al., 2016) where freshwater input is largest, and in the northern AS (Centurioni et al., 2017). Quality-controlled SVP data are made available as 6-hourly interpolated time series (Hansen and Poulain, 1996; Lumpkin and Centurioni, 2019; http://www.aoml.noaa.gov/phod/dac/index.php). If a drifter is drogued, the computed velocity measurements are accurate to about 0.01 m s^{-1} for winds up to 10 m s^{-1} when a wind slip correction is applied (Niiler et al., 1995). However, for this study, velocity data from both drogued and undrogued drifters are used after applying the correction described by Pazan and Niiler (2001) for undrogued drifters.

To compute the time-dependent near-surface currents, the multivariate two-dimensional regression model described in Centurioni et al. (2009) was adapted to use wind stress data instead of wind velocity and a scalar coefficient for the altimetry-derived geostrophic velocity anomaly. The three coefficients of the regression model represent the average unbiased near-surface geostrophic velocity field, a scalar scaling factor for the altimetry-derived geostrophic velocity anomaly and a coefficient that provides a scaling factor and rotation for the wind-driven currents. This formulation is essentially equivalent to the slab model of the upper ocean by Lagerloef et al. (1999), but Centurioni et al. (2009) also provide an analytical solution to the problem. The three regression coefficients mentioned above were computed for the tropical Indian Ocean covering the completed years 1993–2016 after minimizing the cost function described in Centurioni et al. (2009) using three different datasets. The first is the 15-m depth SVP drifter velocity dataset. The second one is the sea level anomaly (SLAs) and associated geostrophic velocity anomaly from the delayed-time multi-mission product provided by the Copernicus Marine Environment Monitoring Service (CMEMS; http://marine.copernicus.eu), available as daily global maps, including the equatorial region, with respect to a 20-year mean (1993–2012) on a regular 0.25° x 0.25° horizontal grid since January 1993 (Ducet et al., 2000). The third dataset represents the wind stress field derived from the COARE (Coupled Ocean-Atmosphere Response Experiment) 3.5 algorithm (Edson et al., 2013) using 6-hourly ECMWF (European Centre for Medium-Range Weather Forecasts; https://www.ecmwf.int) ERA-Interim winds with a spatial resolution of 0.75° (Dee et al., 2011). As could be expected, the region around the equator needs special handling. The wind-driven current coefficient, which essentially describes the Ekman currents at a characteristic depth, fails to produce realistic results within five degrees of the equator. Following the same procedure introduced by Lagerloef et al. (1999), such coefficient was reconstructed by interpolating the vertical viscosity and characteristic depth of the slab model in the 5°S - 5°N region using a two-dimensional cubic interpolant. Finally, the explained variance of the slab model was used to identify regions where the other two regression coefficients, namely the average unbiased velocity field and the scalar scaling factor for the altimetry-derived geostrophic velocity anomaly, were ill-defined. It was observed that this typically occurs within two degrees of the equator, where the explained variance drops below 0.6. The associated values for the unbiased velocity field and the altimetry scaling factor were therefore discarded and the interpolated values computed from the same two-dimensional cubic interpolant were used instead. The computations were performed on a 1.5° x 1.5° horizontal grid due to the availability of drifter data and subsequently interpolated to a 0.25° spatial resolution. Time-dependent geostrophic and Ekman velocity fields as well as seasonal averages were reconstructed using the CMEMS and COARE daily fields, with averages computed over the period 1993–2016. This product is hereafter referred to as drifter/altimetry/wind synthesis.

2.2. Argo floats

Quality-controlled temperature and salinity profiles within the tropical Indian Ocean for the period 2004–2016 were obtained from the NOAA (National Oceanic and Atmospheric Administration) National Centers for Environmental Information, Global Argo Data Repository (GADR; https://www.nodc.noaa.gov/argo/), with salinity observations targeting a long-term accuracy of 0.01 psu (e.g. Riser et al., 2008). The distribution of Argo observations that fall within specific ranges of density sigma-0/salinity (σ_0/S) space were mapped for data below 20 m to reduce the signature of the immediate surface layer subject to local weather. Argo temperature and salinity profiles were used if they had five or more data points within the following designated σ_0/S boxes: AS waters of $\sigma_0 < 24$ (A_1) and $\sigma_0 < 23.25$ (A_2) as well as BoB waters of $\sigma_0 < 21.5$ (B_1) and $\sigma_0 < 22$ (B_2). As the Argo floats are not distributed uniformly in space and time, the mapped distributions do not necessarily represent mean climatological conditions.

2.3. Ancillary data

SSS data from the JPL (Jet Propulsion Laboratory) SMAP-SSS V4.2 CAP (daily 8-day running mean, level 3; Fore et al., 2016; https://doi.org/10.5067/SMP42-3TPCS) product from NASA's (National Aeronautics and Space Administration) SMAP (Soil Moisture Active Passive) observatory are also used in this study. The dataset is based on the JPL CAP (Combined Active-Passive) retrieval algorithm and available on a 0.25° x 0.25° grid since April 2015. Validation of SMAP SSS with in situ measurements has indicated an accuracy of 0.2 psu in the tropics and mid-latitudes on a monthly basis and L3 daily maps can resolve high-salinity water intrusions from the AS into the BoB during the Indian summer monsoon (Tang et al., 2017).

3. Results

The seasonal (i.e. boreal winter: December-January-February; boreal spring: March-April-May; boreal summer: June-July-August; boreal fall: September-October-November) export pathways of freshwater out of the BoB can be illustrated by historical drifter trajectories overlaid on SSS (Fig. 2), which were compiled using only locations from drogued drifters to maximize the Lagrangian aspect of the dataset. For this purpose, we exclusively selected drifters within the BoB (i.e. > 3.75°N, > 80°E) during each season independent of year and their tracks were plotted throughout the end of their lifetime which can be well beyond the respective season. During the winter northeast monsoon (Fig. 2a), the drifter trajectories clearly confirm the existence of an export route around the southern rim of Sri Lanka which is also apparent in the preceding boreal-fall intermonsoon period (Fig. 2d; e.g. Lee et al., 2016). Previous studies have described a connected wintertime surface current system south of Sri Lanka, continuing northward along the west coast of India (e.g. Schott and McCreary, 2001; Schott et al., 2009). However, none of the drifters contained in the

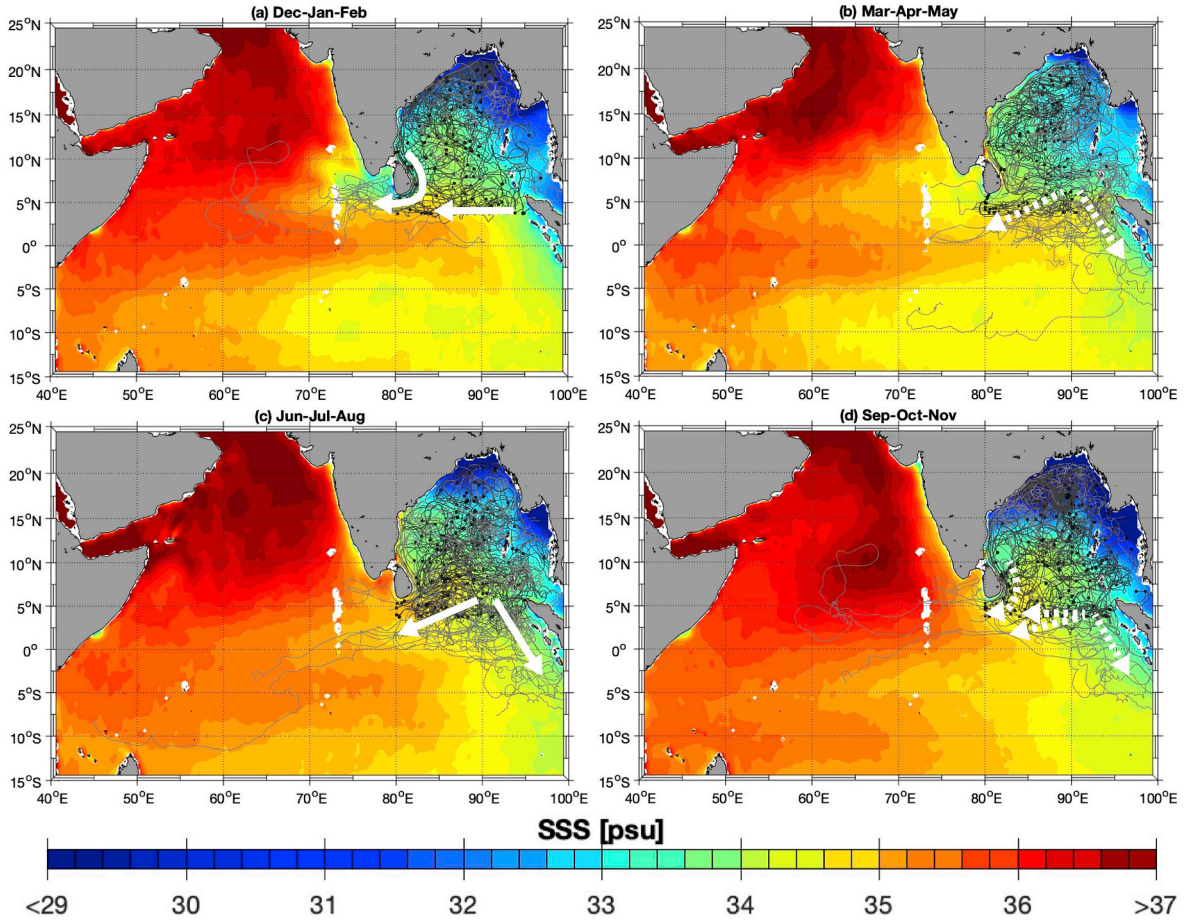

Fig. 2. Seasonal evolution of drogued drifter trajectories from the historical GDP archive starting within the BoB (i.e. > 3.75°N, > 80°E; black symbols mark the first drifter positions for each season and dark gray lines illustrate the drifter trajectories during the season shown in each panel while light gray lines indicate the trajectories after that season) overlaid on 4-year mean SMAP SSS maps (color): (a) December-January-February (N = 150), (b) March-April-May (N = 132), (c) June-July-August (N = 189), and (d) September-October-November (N = 228). (Dashed) white arrows indicate export pathways out of the BoB during the (inter-) monsoon periods. (For interpretation of the references to color in this figure legend, the reader is referred to the Web version of this article.)

historical GDP archive including recent ONR deployments in critical regions exits the BoB and continues northward along the west coast of India in boreal winter, indicating that there is little connectivity between the surface flow south of Sri Lanka and along the west coast of India. It should also be noted that both the drifter tracks and the SSS distributions in boreal fall and spring suggest that the near-surface westward flow is blocked by the Maldives Island chain, where presumably intense stirring/mixing occurs. During the boreal-spring transition phase (Fig. 2b), the drifter trajectories indicate the occurrence of cross-equatorial pathways which become more evident in boreal summer and fall (Fig. 2c,d; e.g. Sengupta et al., 2006) when many drifters spread southward in the eastern tropical Indian Ocean in areas characterized by comparatively low SSS. Several drifters also move westward near the equator during both the summer southwest monsoon and boreal-fall intermonsoon periods. In summary, the BoB drifter tracks point to the existence of two distinct near-surface export pathways. It should further be noted that many drifters recirculate in the BoB which may be attributed to a rather sluggish and persistent eddy field within the interior of the BoB (e.g. Hormann et al., 2016; Gordon et al., 2016).

As mentioned in the introduction, saltier water needs to be advected into the BoB to balance this freshwater export and achieve a quasi-steady SSS state. To highlight possible near-surface pathways through which such compensating exchanges of saltier water can occur, drifters starting within the AS (i.e. > 0°, < 80°E) are examined here (Fig. 3). First drifter positions for each season were again identified independent of year and the trajectories were then plotted until the end of each drifter's lifetime. During boreal winter, the drifter tracks indicate an eastward spreading of high-salinity AS water along the equator to about 90°E with hardly any drifter reaching into the BoB and only a few of them crossing the equator southward (Fig. 3a). In the following inter-monsoon period, the dominant pathway is still along the equator but the drifters now show a distinct tendency for crossing it southward (e.g. Jensen, 2003) where they finally get entrained into the westward SEC near 10°S (Fig. 3b). During the summer southwest monsoon, there are clear indications of an additional eastward pathway north of the equator around Sri Lanka that reaches into the BoB (Fig. 3c). Drifters starting in boreal fall also suggest an equatorial advection of AS water into the central BoB and hardly any of them cross the equator to the south (Fig. 3d). In agreement with observations and model results (e.g. Murty et al., 1992; Vinayachandran et al., 1999; Jensen et al., 2016), the historical drogued drifter trajectories corroborate the near-surface spreading of high-salinity surface water from the AS into the BoB as far north as about 10°N. However, it should be noted that the drifters do not trace AS waters when they are subducted in the BoB and the observations from subsurface Argo floats provide additional details in this regard as discussed below.

Eulerian circulation patterns and associated eddy kinetic energy (EKE) fields obtained from the time-dependent near-surface currents computed with the drifter/altimetry/wind synthesis are examined in the context of the pathways suggested by the analysis of the drifter tracks. Seasonal maps of the total near-surface velocities in the tropical

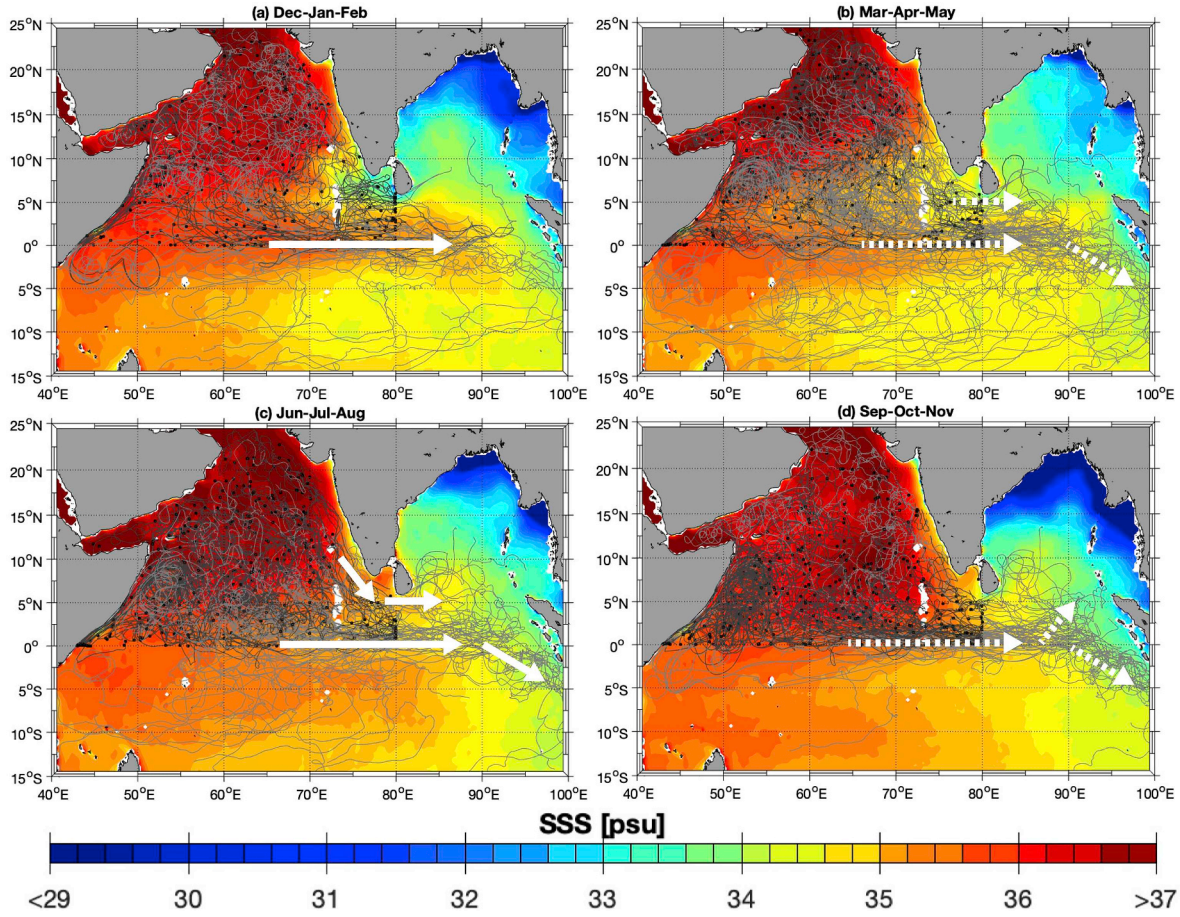

Fig. 3. Same as Fig. 2, but for the AS (i.e. > 0°, < 80°E): (a) December-January-February (N = 255), (b) March-April-may (N = 331), (c) June-July-August (N = 311), and (d) September-October-November (N = 306).

Indian Ocean highlight the prominent features of the regional circulation with its year-round prevailing SEC in the southern hemisphere and annually reversing currents in the two northern embayments (Fig. 4; e.g. Schott and McCreary, 2001; Schott et al., 2009). Most notably, the Somali Current (SC) along the western boundary of the AS flows northward (southward) during the southwest (northeast) monsoon and the monsoon current south of Sri Lanka also switches direction from eastward in boreal summer to westward in boreal winter with the reversal of the wind system (Fig. 4a,c). During the two intermonsoon periods in boreal spring and fall, there are indications of the eastward Wyrtki Jets along the equator (Wyrtki, 1973) with the latter being more pronounced (Fig. 4b,d). Except for the SEC, the above current systems are all associated with large EKE ($\boldsymbol{EKE} = \frac{\boldsymbol{u}'^2 + \boldsymbol{v}'^2}{2}$, where $\boldsymbol{u}'$ and $\boldsymbol{v}'$ are the zonal and meridional velocity anomalies, respectively) and enhanced values are also found in the EICC region along the east Indian coast during the intermonsoon periods (Fig. 4; e.g. Shenoi et al., 1999; Peng et al., 2015). In agreement with previous observations (e.g. Durand et al., 2009), the EICC does not appear as a continuous flow and shows pronounced spatiotemporal variability due to mesoscale eddies. The distinct eddy variability in interbasin exchange regions such as around Sri Lanka is expected to affect the freshwater export out of the BoB, where interior currents and associated EKE are generally weak throughout the year.

Focusing on the near-surface currents in the critical interbasin exchange regions south of Sri Lanka and across the southern BoB (locations indicated by black solid lines in Fig. 1), Fig. 5 shows the velocity vectors of the total, geostrophic, and Ekman currents along 81°E and 8°N for the southwest and northeast monsoon seasons as derived from the drifter/altimetry/wind synthesis. South of Sri Lanka and north of about 3°N, the flow is dominated by the westward NMC in boreal winter (Fig. 5a) and the eastward SMC in boreal summer (Fig. 5b). While the wintertime NMC is largely in geostrophic balance, the summertime SMC also exhibits considerable Ekman contributions (e.g. Shankar et al., 2002) which extend and dominate the total flow farther south and near the equator where the wind-driven flow is approximately in the direction of the wind. In summary, the meridional transect along 81°E clearly supports the existence of and quantifies persistent interbasin exchange pathways of opposite direction during the northeast and southwest monsoons. Contrary to the strong zonal currents south of Sri Lanka, the velocity vectors along 8°N are largely meridionally oriented during both monsoon seasons (Fig. 5c,d). The most prominent circulation features along this transect across the southern BoB are the southward EICC to the east of Sri Lanka in boreal winter (i.e. $\sim$0.30 m s^{-1}; Fig. 5c) and acyclonic gyre - the Sri Lanka Dome - in boreal summer (i.e. < 86°E; Fig. 5d). Both features are largely in geostrophic balance and the latter involves a southward coastal current of comparable strength to the EICC (i.e. $\sim$0.25 m s^{-1}). On the other hand, the seasonal near-surface velocities are generally weaker in the interior of the BoB during both the northeast and southwest monsoon where Ekman currents are northward (southward) in boreal winter (summer). However, the zonal transect along 8°N confirms the known near-surface freshwater export pathway along the eastern boundary of the BoB during both monsoon seasons (e.g. Behara and Vinayachandran, 2016). While there is a narrow but strong southward current (i.e. > 97°E; $\sim$0.25 m s^{-1}) in boreal winter, the flow is broader and weaker (i.e. > 95°E; $\sim$0.15 m s^{-1}) in boreal summer. Overall the results of this zonal transect across the southern BoB are in qualitative agreement with a recent model study by Jensen et al. (2016).

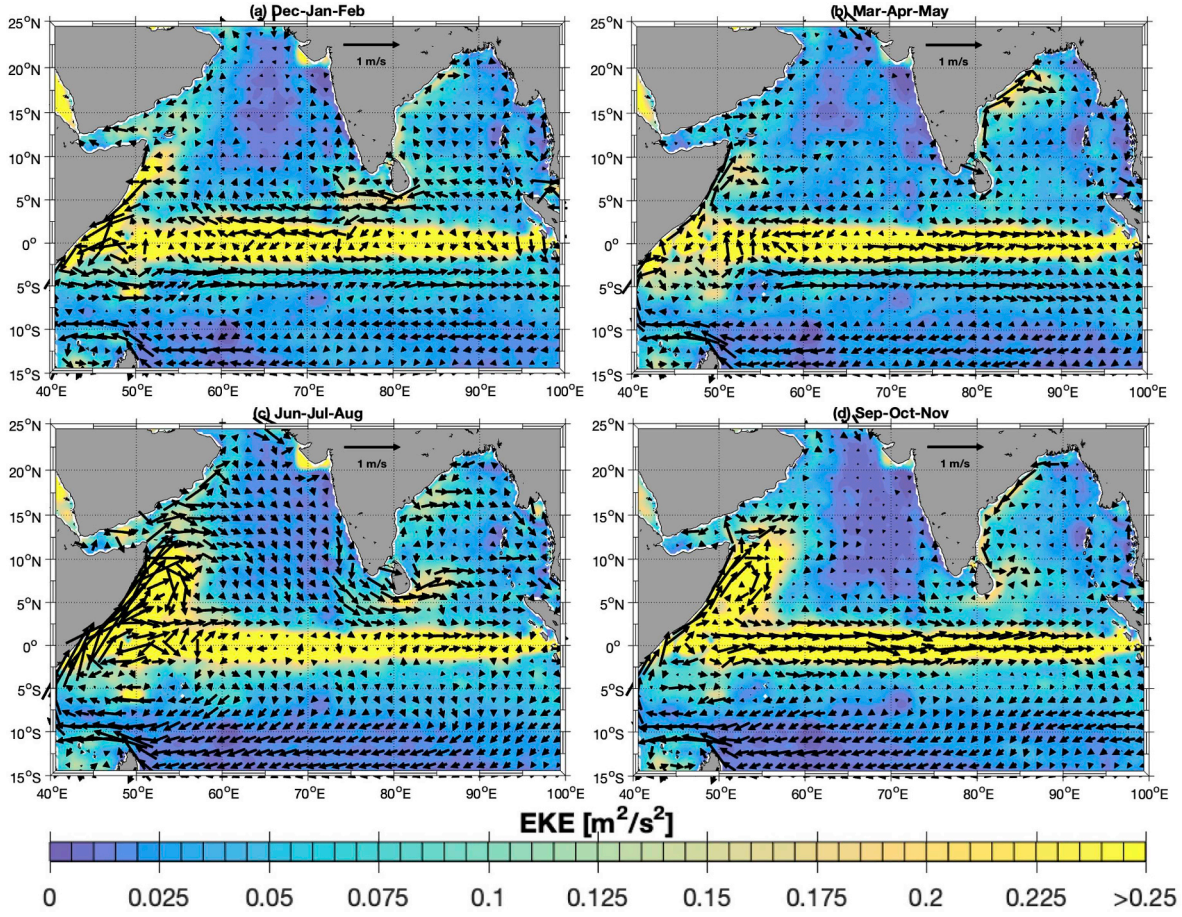

Fig. 4. Seasonal maps of total near-surface currents from the drifter/altimetry/wind synthesis for the period 1993–2016 (black vectors; 1.5° spatial resolution only) overlaid on corresponding EKE distributions (color): (a) December-January-February, (b) March-April-May, (c) June-July-August, and (d) September-October-November. (For interpretation of the references to color in this figure legend, the reader is referred to the Web version of this article.)

To elucidate further details of the eastern export route, Fig. 6 shows the seasonal near-surface currents along 6.5°N (location indicated by black solid line in Fig. 1) separated into total, geostrophic, and Ekman velocity components from the drifter/altimetry/wind synthesis. Although the southward currents across this transect are generally weak (i.e. of the order of a few cm s^{-1}), there are clear indications for a year-round export of freshwater between about 90°E and 91°E. The largest negative meridional velocities occur during the summer southwest monsoon (i.e. up to ~0.1 m s^{-1}) when the near-surface currents are primarily wind-driven and the longitudinal export range extends to about 93.5°E (Fig. 6c). These observations are in general agreement with previous studies suggesting that the eastern boundary path is most pronounced during the second half of the year (e.g. Benshila et al., 2014; Behara and Vinayachandran, 2016). It should also be noted that there is a year-round northward current at the eastern end of this transect which is largely in geostrophic balance.

Further insight into the interbasin exchange pathways in the tropical Indian Ocean is provided by temperature and salinity profiles obtained from Argo floats. Argo data within the two embayments of the Indian Ocean north of 8°N reveal the remarkably different stratification characteristics between the salty AS and the fresher BoB (Fig. 7, upper σ_o/S panel). The Argo observations are used to trace the spreading of AS and BoB waters of $\sigma_0 < 24$ for the AS (i.e. upper ~100 m on average) and $\sigma_0 < 22$ for the BoB (i.e. upper ~75 m on average). Within the σ_0/S scatter boxes, A_1 and B_1 represent the more extreme AS and BoB salinity ranges, respectively (Fig. 7, lower left panels). The A_1 water spreads south of 8°N approaching the equator, with some penetration to the east of the Maldives Island chain. On the other hand, the B_1 water spreads to the south of 8°N along two pathways: around the southern rim of Sri Lanka into the AS southeast corner, and with a more dominant presence along the western margin of Sumatra. A more pervasive spreading of AS and BoB waters is seen in the σ_0/S boxes A_2 and B_2 representing more diluted versions of AS and BoB waters, respectively (Fig. 7, lower right panels). Eastward extension of the A_2 water is primarily observed between 0° and 4°N within the boreal-summer axis of the South Equatorial Counter Current (SECC) as well as along the southern rim of Sri Lanka within the SMC (e.g. Schott and McCreary, 2001; Schott et al., 2009). This AS water further penetrates into the central BoB, spreading within the upper thermocline as a salinity maximum to mix into the surface water countering the excessive boreal-summer freshwater inflow (e.g. Vinayachandran et al., 2013; Gordon et al., 2016). The BoB B_2 water is pervasive throughout the eastern tropical Indian Ocean, spreading southward along the western margin of Sumatra as well as leaching into the interior - presumably within the NMC south of Sri Lanka during boreal winter, which occupies a wide latitudinal range as the SECC shifts to the south of the equator (e.g. Beal et al., 2013). The westward spreading south of Sri Lanka reaches into and beyond the Maldives Island chain into the AS, while the B_2 water spreads along the western margin of Sumatra as far south as the westward spreading ITF plume near 10°S (e.g. Gordon et al., 1997).

4. Discussion

The analysis of historical drifter trajectories in the tropical Indian Ocean has highlighted the occurrence and quantified the surface expression of two distinct freshwater export pathways from the BoB as

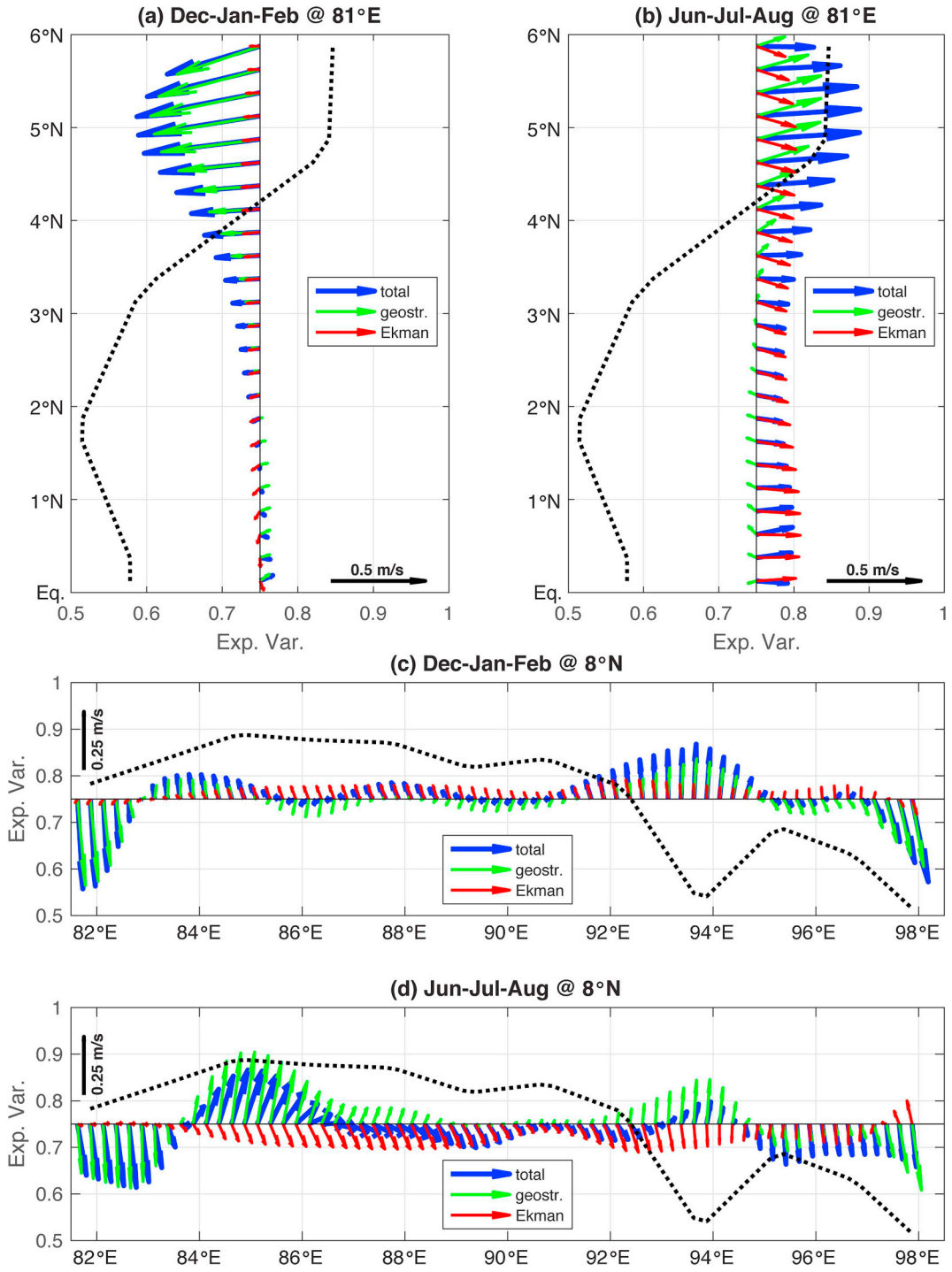

Fig. 5. Transects of near-surface currents along (a, b) 81°E and (c, d) 8°N (cf. Fig. 1, black solid lines) for (a, c) December-January-February and (b, d) June-July-August separated into total (blue), geostrophic (green), and Ekman (red) velocity components from the drifter/altimetry/wind synthesis for the period 1993–2016; current vectors are given with respect to the x-axis (i.e. representing actual current directions). Dotted black lines indicate the explained variance of the drifter/altimetry/wind synthesis (i.e. correlation between altimetry- and drifter-derived geostrophic velocity anomalies). (For interpretation of the references to color in this figure legend, the reader is referred to the Web version of this article.)

well as the advection of saltier AS water into the BoB from both Lagrangian (cf. Figs. 2 and 3) and Eulerian (cf. Figs. 5 and 6) perspectives. The seasonal monsoon currents around Sri Lanka are of importance as they provide a mechanism for a direct interbasin exchange of waters between the BoB and AS (Fig. 8). East of Sri Lanka the flow is dominated by the southward EICC during the winter northeast monsoon which feeds into the westward NMC and hence provides an export route for low-salinity BoB water (Fig. 8a). There are also indications of the so-called Laccadive High off the southwest coast of India in boreal winter (i.e. ~7.5°N, 74.5°E) that may hamper the spreading of this freshwater into the eastern AS against earlier conclusions (e.g. Bruce et al., 1994; Schott and McCreary, 2001). Otherwise, its counterpart - the Laccadive Low - which has been suggested to be involved in the supply of the eastward SMC south of Sri Lanka is not apparent in our analysis during the summer southwest monsoon (Fig. 8b; e.g. Shankar et al., 2002). Farther east, the summertime SMC splits into two

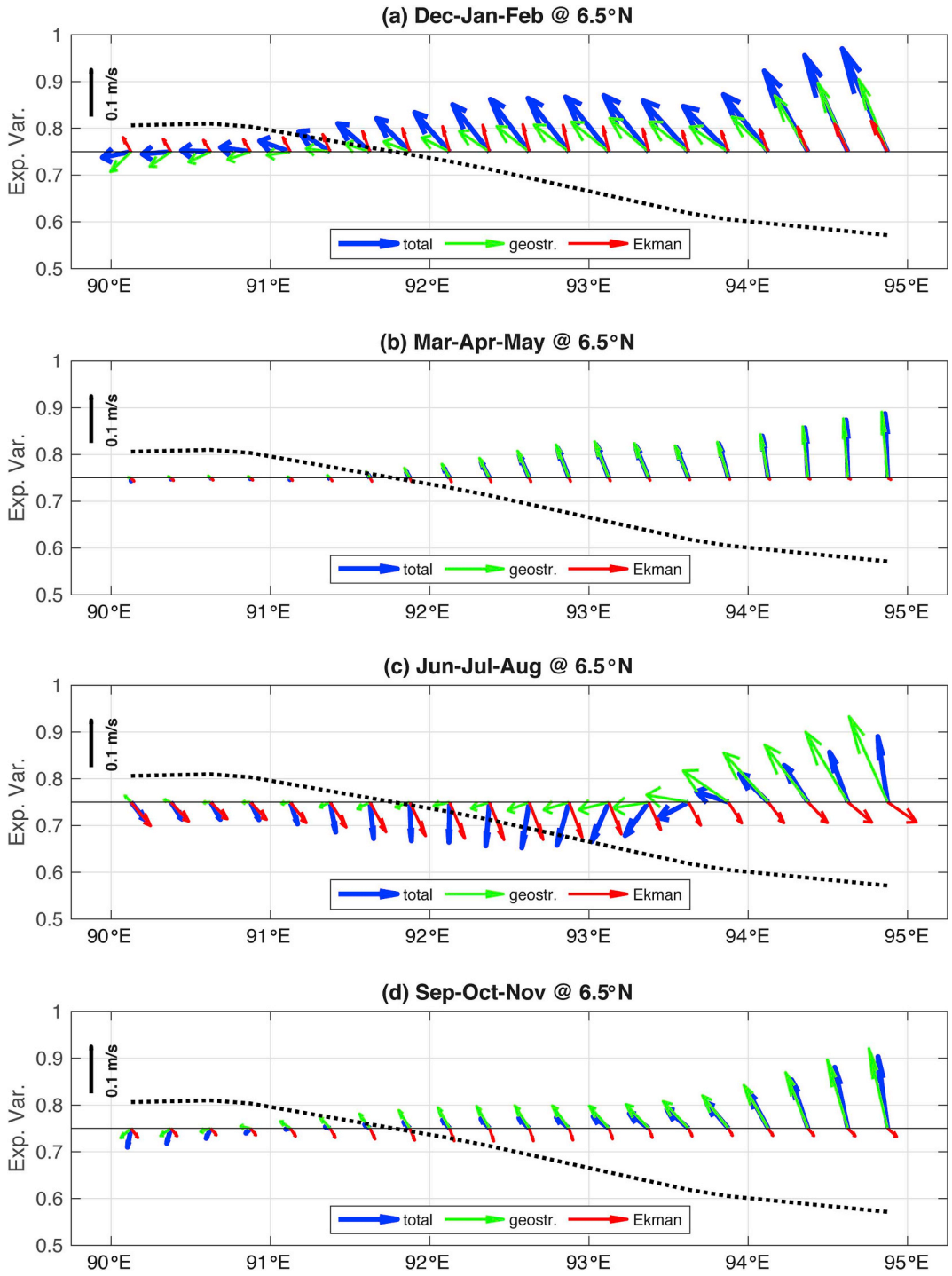

Fig. 6. Same as Fig. 5, but along 6.5°N (cf. Fig. 1, black solid line) and for all seasons: (a) December-January-February, (b) March-April-May, (c) June-July-August, and (d) September-October-November.

branches: one continues eastward and the other one turns northeastward into the BoB. Driven by the wind stress curl associated with the southwest monsoon, the Sri Lanka Dome develops in this region (e.g. Vinayachandran and Yamagata, 1998) which involves a southward coastal current as in boreal winter (Fig. 8). However, the associated freshwater flow encounters here saltier AS water entering the BoB within the upper thermocline that leads to a pronounced front in the critical interbasin exchange region around Sri Lanka (e.g. Gordon et al., 2016; Lee et al., 2016).

Although the mean seasonal flow south of Sri Lanka is dominantly eastward during the southwest monsoon, a corresponding zonal velocity time series at 5.5°N indicates instances of westward flow between the SMC and the Sri Lankan coast (Fig. 9; e.g. in 1995, 2005, 2016) as first described by Schott et al. (1994). It has been shown that remote forcing from the equator plays an important role in understanding the variability of the monsoon currents around Sri Lanka (e.g. McCreary et al., 1993; Vinayachandran and Yamagata, 1998) and an equatorial Rossby wave is observed to radiate westward from the eastern boundary during the southwest monsoon as exemplified here along 5.5°N for the year 2016 (Fig. 10a; location indicated by the black dotted line in Fig. 1). Schott et al. (1994) suggested that the arrival of such a wave south of Sri Lanka can cause a meridional migration of the

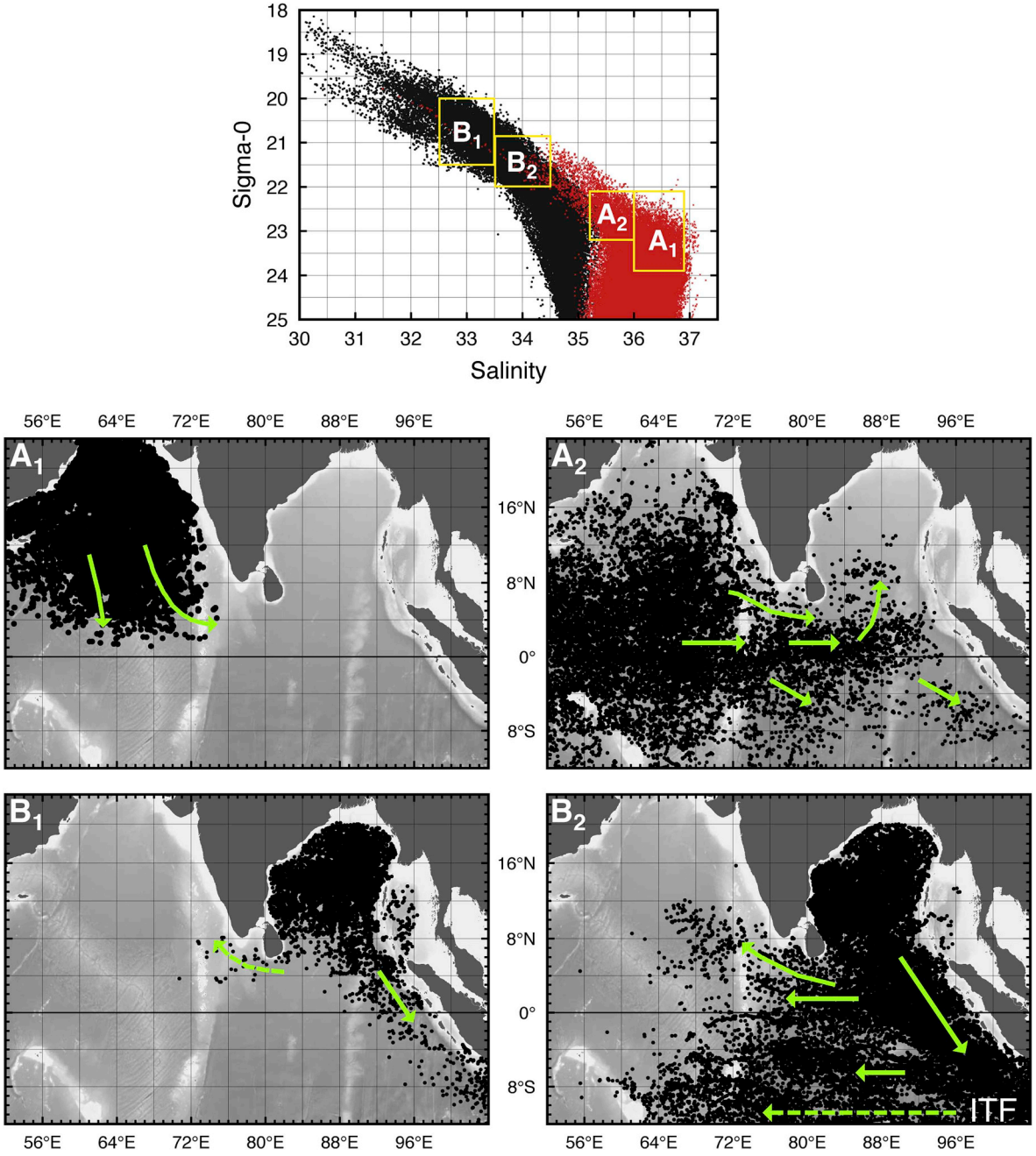

Fig. 7. (Upper panel) sigma-0/salinity (σ_0/S) scatter constructed from Argo floats within the AS (red) and BoB (black) north of 8°N for the period 2004–2016. (Lower panels) Positions of Argo observations falling within the σ_0/S boxes A_1 and A_2 in the AS (first row) as well as B_1 and B_2 in the BoB (second row), which represent water above ~100 m marking the mixed layer and upper thermocline. Green arrows on the maps indicate the spreading pathways out of the AS and BoB, and the dashed green arrow marks the westward spreading of the ITF. (For interpretation of the references to color in this figure legend, the reader is referred to the Web version of this article.)

SMC and Vinayachandran and Yamagata (1998) further attributed Rossby wave propagation for the intrusion of the SMC into the BoB (cf. Fig. 8b). In addition to the radiated Rossby wave, the incident equatorial Kelvin wave partly continues along the rim of the BoB as a coastal Kelvin wave which could provide an explanation for the observed westward flow if it would be a regular phenomenon during the southwest monsoon (Schott et al., 1994). However, our velocity time series south of Sri Lanka clearly shows the intermittency of the westward flow in boreal summer (Fig. 9) which could be caused by sporadically generated coastal Kelvin waves such as through monsoon breaks over the BoB (Schott et al., 1994). A time-longitude diagram of SSS just south of Sri Lanka along 5.5°N further reveals the expected east-west SSS gradient consistent with high-salinity AS water compared to low-salinity BoB water and indicates occasional flow reversals and the occurrence of BoB freshwater south of Sri Lanka at 81°E in boreal summer 2016 (Fig. 10b; location indicated by the black dotted line in Fig. 1). Thus, our observations suggest that besides near-surface advection of saltier AS water into the BoB intermittent flow reversals due to equatorial wave processes can also cause leakage of low-salinity water out of the BoB during the summer southwest monsoon.

5. Summary and conclusions

In this study, drogued drifter and Argo float observations as well as

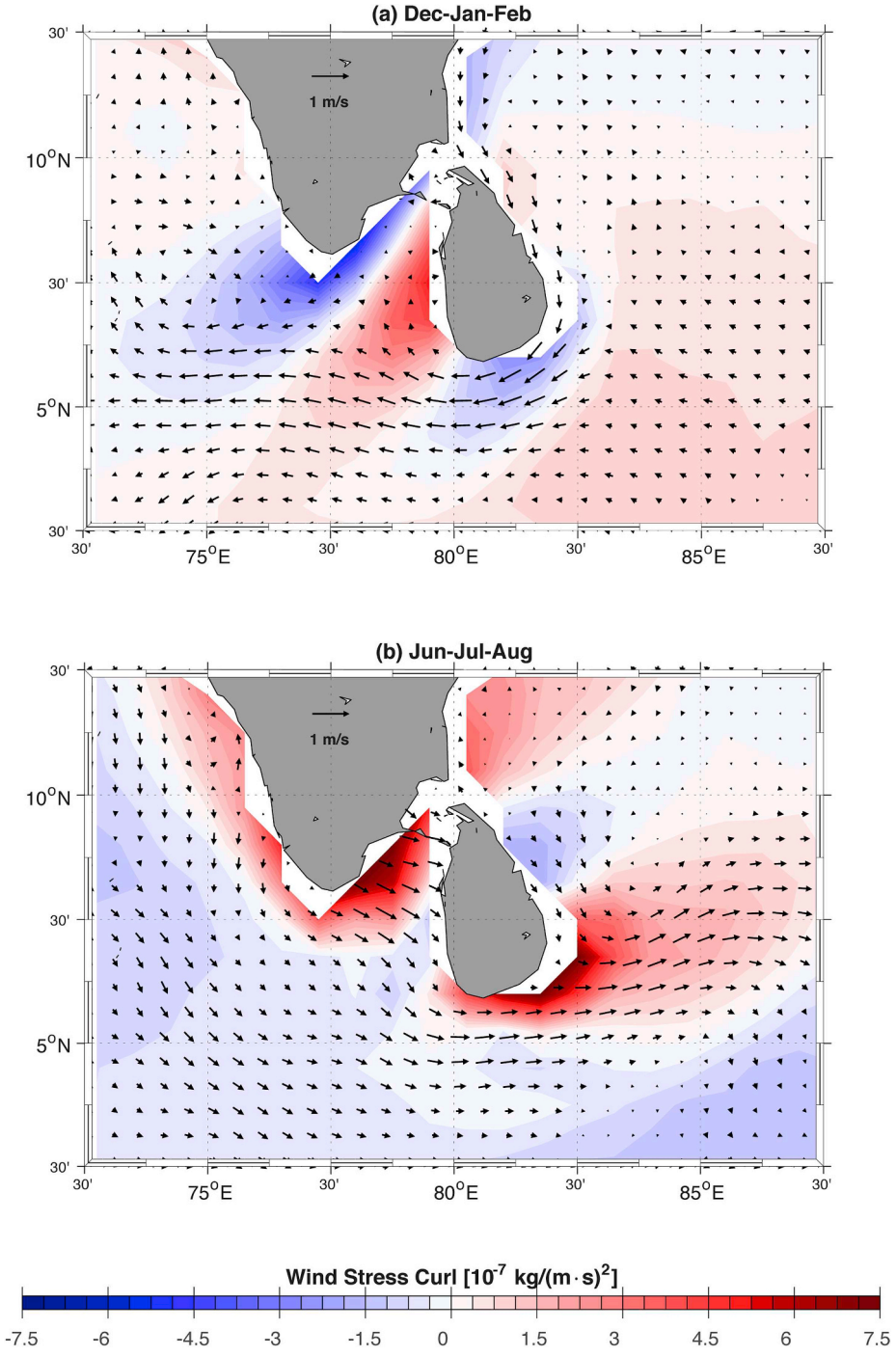

Fig. 8. Maps of total near-surface currents around Sri Lanka from the drifter/altimetry/wind synthesis for the period 1993–2016 (black vectors; 0.5° spatial resolution only) overlaid on corresponding COARE wind stress curl distributions (color): (a) December-January-February, and (b) June-July-August. (For interpretation of the references to color in this figure legend, the reader is referred to the Web version of this article.)

a synthesis of drifters, satellite altimetry, and wind stress forcing have been used to investigate details of the freshwater export pathways from the BoB and the balancing inflow of saltier AS water into the BoB. These datasets confirm the existence of two main export routes out of the BoB, one along the east coast of India and around Sri Lanka and the other along its eastern boundary. While the former prevails during the winter northeast monsoon, the latter gains in importance toward the boreal summer and fall seasons. The critical interbasin exchange region around Sri Lanka has further been found to be affected by mesoscale eddies, implying that the wintertime freshwater export out of the BoB is associated with large variability which may be modulated by equatorial wave processes (e.g. McCreary et al., 1993; Vinayachandran and Yamagata, 1998). The drifter data available to date do not support the notion of a continuous current system comprised of the westward NMC south of Sri Lanka and the West India Coastal Current (WICC) around the Laccadive High in boreal winter (e.g. Schott and McCreary, 2001; Schott et al., 2009) that can directly export surface freshwater from the BoB to the AS. The drifter tracks and SSS maps rather suggest a blocking effect of the Maldives Island chain, which may imply that the surface water is locally stirred and/or mixed by flow - topography interaction processes. As first described by Schott et al. (1994), our observations additionally indicate an occasional leakage of low-salinity water by a

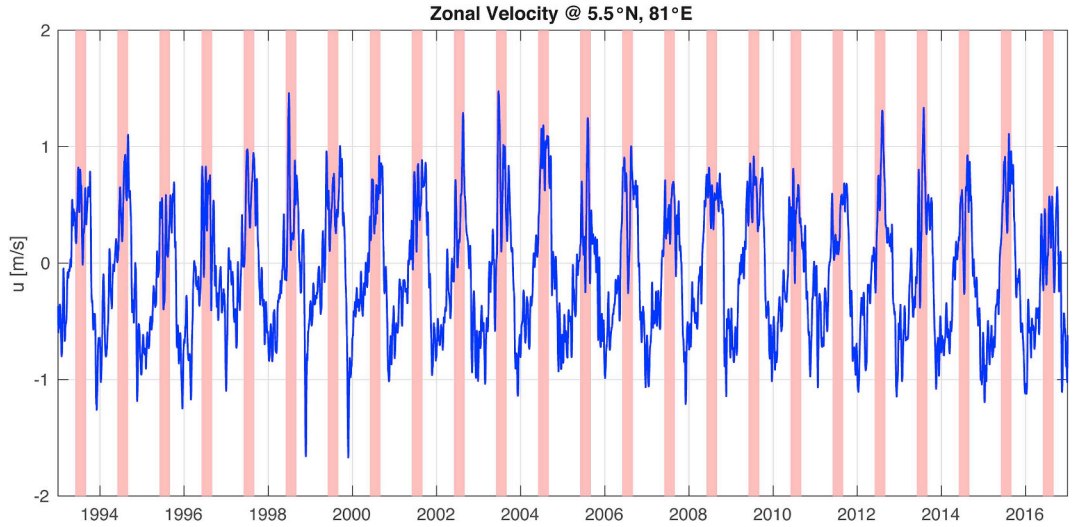

Fig. 9. Total zonal velocity (i.e. positive: eastward; negative: westward) time series from the drifter/altimetry/wind synthesis for the period 1993–2016 smoothed by a weekly running mean at 5.5°N, 81°E where light red bars mark boreal summer. (For interpretation of the references to color in this figure legend, the reader is referred to the Web version of this article.)

westward coastal current between the eastward SMC and Sri Lanka during the summer southwest monsoon. Although this flow has also been simulated by numerical models (e.g. Vinayachandran and Yamagata, 1998), it has not received much attention and the drifter/altimetry/wind synthesis provides the first long-term observations of this intermittent westward current. The summertime SMC facilitates the transport of saltier AS water into the BoB and exhibits considerable Ekman contributions in contrast to the geostrophically-balanced westward NMC in boreal winter. Idealized model experiments have shown that the advection of high-salinity AS water within the SMC can alter the evolution of temperature and salinity in the BoB, which could potentially affect Indian monsoon rainfall (Webber et al., 2018). Tracing the spreading of the remarkably different AS and BoB waters in the mixed layer and upper thermocline by subsurface Argo floats has not only revealed the intrusion of high-salinity AS water into the BoB but also the export of freshwater out of the BoB around Sri Lanka and along the western margin of Sumatra as far south as the ITF plume near 10°S where it flows westward within the SEC. Upon reaching the western boundary of the tropical Indian Ocean, some of this low-salinity water turns northward into the AS (e.g. Gordon et al., 1997).

To conclude, this study has shed new light on the two spreading pathways of excess freshwater from the BoB into the tropical Indian Ocean and AS indicating that the year-round export path along the eastern boundary may be dominant from an annual perspective compared to the highly seasonal pathway in the western BoB. Quantification of these observational results invites comparisons to

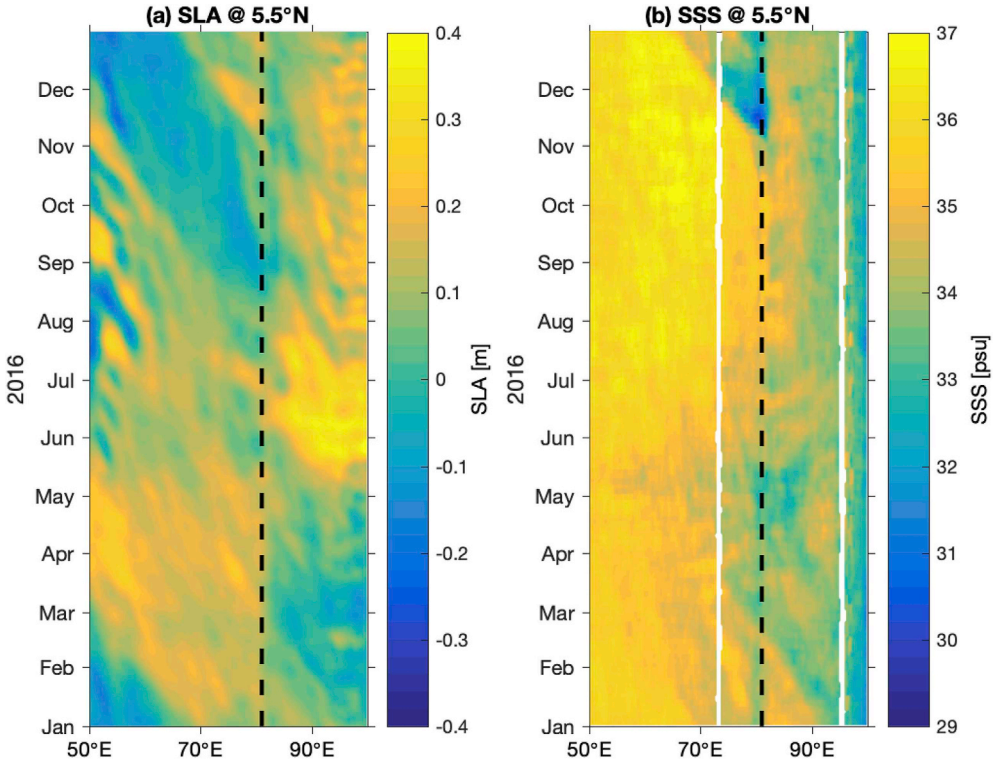

Fig. 10. Longitude-time diagrams of (a) CMEMS SLA and (b) SMAP SSS along 5.5°N for the year 2016; black dashed lines mark 81°E (cf. Fig. 1, black dotted line).

numerical models.

Acknowledgements

This study was supported by ONR grants N00014-13-1-0477 (VH and LC), N00014-14-1-0183 (VH and LC), N00014-15-1-2286 (VH and LC), and N00014-16-1-2480 (AG) as well as NOAA GDP grant NA15OAR4320071 (VH and LC). We would like to thank Tommy Jensen and an anonymous reviewer for their comments that helped to improve the manuscript. Declarations of interest: none. Lamont-Doherty Earth Observatory contribution number 8353.

References

Akhil, V.P., Lengaigne, M., Vialard, J., Durand, F., Keerthi, M.G., Chaitanya, A.V.S., Papa, F., Gopalakrishna, V.V., de Boyer Montégut, C., 2016. A modeling study of processes controlling the Bay of Bengal sea surface salinity interannual variability. J. Geophys. Res. – Oceans 121, 8471–8495. https://doi.org/10.1002/2016JC011662.

Beal, L.M., Hormann, V., Lumpkin, R., Foltz, G.R., 2013. The response of the surface circulation of the Arabian Sea to monsoonal forcing. J. Phys. Oceanogr. 43, 2008–2022. https://doi.org/10.1175/JPO-D-13-033.1.

Benshila, R., Durand, F., Masson, S., Bourdallé-Badie, R., de Boyer Montégut, C., Papa, F., Madec, G., 2014. The upper Bay of Bengal salinity structure in a high-resolution model. Ocean Model. 74, 36–52. https://doi.org/10.1016/j.ocemod.2013.12.001.

Behara, A., Vinayachandran, P.N., 2016. An OGCM study of the impact of rain and river water forcing on the Bay of Bengal. J. Geophys. Res. – Oceans 121, 2425–2446. https://doi.org/10.1002/2015JC11325.

Bruce, J.G., Johnson, D.R., Kindle, J.C., 1994. Evidence for eddy formation in the eastern Arabian Sea during the northeast monsoon. J. Geophys. Res. – Oceans 99 (C4), 7651–7664.

Centurioni, L.R., 2018. Drifter technology and impacts for sea surface temperature, sea-level pressure, and ocean circulation studies. In: Venkatesan, R., Tandon, A., D'Asaro, E., Atmanand, M.A. (Eds.), Observing the Oceans in Real Time. Springer Oceanography, Cham, Switzerland, pp. 37–58. https://doi.org/10.1007/978-3-319-66493-4_3. Springer International Publishing AG.

Centurioni, L.R., Hormann, V., Talley, L.D., Arzeno, I., Beal, L., Caruso, M., et al., 2017. Northern Arabian Sea Circulation – autonomous research (NASCar): a research initiative based on autonomous sensors. Oceanography 30 (2), 74–87. https://doi.org/10.5670/oceanog.2017.224.

Centurioni, L.R., Niiler, P.N., Lee, D.-K., 2009. Near-surface circulation in the South China Sea during the winter monsoon. Geophys. Res. Lett. 36, L06605. https://doi.org/10.1029/2008GL037076.

Dee, D.P., Uppala, S.M., Simmons, A.J., Berrisford, P., Poli, P., Kobayashi, S., et al., 2011. The ERA-Interim reanalysis: configuration and performance of the data assimilation system. Q. J. Roy. Meteor. Soc. 137, 553–597.

Ducet, N., Le Traon, P.Y., Reverdin, G., 2000. Global high-resolution mapping of ocean circulation from TOPEX/Poseidon and ERS-1 and -2. J. Geophys. Res. – Oceans 105 (C8), 19477–19498.

Durand, F., Shankar, D., Birol, F., Shenoi, S.S.C., 2009. Spatiotemporal structure of the East India Coastal Current from satellite altimetry. J. Geophys. Res. – Oceans 114, C0213. https://doi.org/10.1029/2008JC004807.

Edson, J.B., Jampana, V., Weller, R.A., Bigorre, S.P., Plueddemann, A.J., Fairall, C.W., et al., 2013. On the exchange of momentum over the open ocean. J. Phys. Oceanogr. 43, 1589–1610. https://doi.org/10.1175/JPO-D-12-0173.1.

Fore, A.G., Yueh, S.H., Tang, W., Stiles, B.W., Hayashi, A.K., 2016. Combined active/passive retrievals of ocean vector wind and sea surface salinity with SMAP. IEEE T. Geosci. Remote 54 (12), 7396–7404. https://doi.org/10.1109/TGRS.2016.2601486.

Gordon, A.L., Ma, S., Olson, D.B., Hacker, P., Ffield, A., Talley, L.D., Wilson, D., Baringer, M., 1997. Advection and diffusion of Indonesian throughflow water within the Indian Ocean South Equatorial Current. Geophys. Res. Lett. 24 (21), 2573–2576.

Gordon, A.L., Shroyer, E.L., Mahadevan, A., Sengupta, D., Freilich, M., 2016. Bay of Bengal: 2013 northeast monsoon upper-ocean circulation. Oceanography 29 (2), 82–91. https://doi.org/10.5670/oceanog.2016.41.

Hansen, D.V., Poulain, P.-M., 1996. Quality control and interpolations of WOCE-TOGA drifter data. J. Atmos. Ocean. Technol. 13, 900–909.

Hastenrath, S., Greischar, L., 1991. The monsoonal current regimes of the tropical Indian Ocean: observed surface flow fields and their geostrophic and wind-driven components. J. Geophys. Res. – Oceans 96 (C7), 12619–12633.

Hormann, V., Centurioni, L.R., Mahadevan, A., Essink, S., D'Asaro, E.A., Praveen Kumar, B., 2016. Variability of near-surface circulation and sea surface salinity observed from Lagrangian drifters in the northern Bay of Bengal during the waning 2015 southwest monsoon. Oceanography 29 (2), 124–133. https://doi.org/10.5670/oceanog.2016.45.

Jensen, T.G., 2001. Arabian Sea and Bay of Bengal exchange of salt and tracers in an ocean model. Geophys. Res. Lett. 28 (20), 3967–3970.

Jensen, T.G., 2003. Cross-equatorial pathways of salt and tracers from the northern Indian Ocean: modelling results. Deep-Sea Res. II 50, 2111–2127.

Jensen, T.G., 2007. Wind-driven response of the northern Indian Ocean to climate extremes. J. Clim. 20, 2978–2993. https://doi.org/10.1175/jcli4150.1.

Jensen, T.G., Wijesekera, H.W., Nyadjro, E.S., Thoppil, P.G., Shriver, J.F., Sandeep, K.K., Pant, V., 2016. Modeling salinity exchanges between the equatorial Indian Ocean and the Bay of Bengal. Oceanography 29 (2), 92–101. https://doi.org/10.5670/oceanog.2016.42.

Lagerloef, G.S.E., Mitchum, G.T., Lukas, R.B., Niiler, P.P., 1999. Tropical Pacific near-surface currents estimated from altimeter, wind, and drifter data. J. Geophys. Res. - Oceans 104 (C10), 23313–23326.

Lee, C.M., Jinadasa, S.U.P., Anutaliya, A., Centurioni, L.R., Fernando, H.J.S., Hormann, V., et al., 2016. Collaborative observations of boundary currents, water mass variability, and monsoon response in the southern Bay of Bengal. Oceanography 29 (2), 102–111. https://doi.org/10.5670/oceanog.2016.43.

Lumpkin, R., Centurioni, L., 2019. Global Drifter Program Quality-Controlled 6-hour Interpolated Data from Ocean Surface Drifting Buoys. NOAA National Centers for Environmental Information Dataset. Available from. https://doi.org/10.25921/7ntx-z961.

Maximenko, N., Lumpkin, R., Centurioni, L., 2013. Ocean surface circulation. In: Siedler, G., Griffies, S.M., Gould, J., Church, J.A. (Eds.), Ocean Circulation and Climate: A 21st Century Perspective. Academic Press, Oxford, UK and Amsterdam, The Netherlands, pp. 283–304 International Geophysics 103.

McCreary Jr., J.P., Kundu, P.K., Molinari, R.L., 1993. A numerical investigation of dynamics, thermodynamics and mixed-layer processes in the Indian Ocean. Prog. Oceanogr. 31, 181–244.

Murty, V.S.N., Sarma, Y.V.B., Rao, D.P., Murty, C.S., 1992. Water characteristics, mixing and circulation in the Bay of Bengal during southwest monsoon. J. Mar. Res. 50, 2017–2228.

Niiler, P., 2001. The world ocean surface circulation. In: Siedler, G., Church, J., Gould, J. (Eds.), Ocean Circulation and Climate – Observing and Modelling the Global Ocean. Academic Press, London, UK and San Diego, CA, pp. 193–204 International Geophysics 77.

Niiler, P.P., Sybrandy, A.S., Bi, K., Poulain, P.M., Bitterman, D., 1995. Measurements of the water-following capability of holey-sock and TRISTAR drifters. Deep-Sea Res. I 42 (11/12), 1951–1964.

Pant, V., Girishkumar, M.S., Udaya Bhaskar, T.V.S., Ravichandran, M., Papa, F., Thangaprakash, V.P., 2015. Observed interannual variability of near-surface salinity in the Bay of Bengal. J. Geophys. Res. – Oceans 120, 3315–3329. https://doi.org/10.1002/2014JC010340.

Pazan, S.E., Niiler, P.P., 2001. Recovery of near-surface velocity from undrogued drifters. J. Atmos. Ocean. Technol. 18, 476–489.

Peng, S., Qian, Y.-K., Lumpkin, R., Du, Y., Wang, D., Li, P., 2015. Characteristics of the near-surface currents in the Indian Ocean as deduced from satellite-tracked surface drifters. Part I: pseudo-Eulerian statistics. J. Phys. Oceanogr. 45, 441–458. https://doi.org/10.1175/JPO-D-14-0050.1.

Rao, R.R., Sivakumar, R., 2003. Seasonal variability of sea surface salinity and salt budget of the the mixed layer of the north Indian Ocean. J. Geophys. Res. – Oceans 108 (C1), 3009. https://doi.org/10.1029/2001JC000907.

Rao, R.R., Girish Kumar, M.S., Ravichandran, M., Rao, A.R., Gopalakrishna, V.V., Thadathil, P., 2010. Interannual variability of Kelvin wave propagation in the wave guides of the equatorial Indian Ocean, the coastal Bay of Bengal and the southeastern Arabian Sea during 1993-2006. Deep-Sea Res. I 57, 1–13. https://doi.org/10.1016/j.dsr.2009.10.008.

Riser, S.C., Ren, L., Wong, A., 2008. Salinity in Argo: a modern view of a changing ocean. Oceanography 21, 56–67. https://doi.org/10.5670/oceanog.2008.67.

Schott, F.A., McCreary Jr., J.P., 2001. The monsoon circulation of the Indian Ocean. Prog. Oceanogr. 51, 1–123.

Schott, F., Reppin, J., Fischer, J., 1994. Currents and transport of the monsoon current south of Sri Lanka. J. Geophys. Res. – Oceans 99 (C12), 25127–25141.

Schott, F.A., Xie, S.-P., McCreary Jr., J.P., 2009. Indian Ocean circulation and climate variability. Rev. Geophys. 47, RG1002. https://doi.org/10.1029/2007RG000245.

Sengupta, D., Bharath Raj, G.N., Shenoi, S.S.C., 2006. Surface freshwater from Bay of Bengal runoff and Indonesian Throughflow in the tropical Indian Ocean. Geophys. Res. Lett. 33, L22609. https://doi.org/10.1029/2006GL027573.

Shankar, D., Vinayachandran, P.N., Unnikrishnan, A.S., 2002. The monsoon currents in the north Indian Ocean. Prog. Oceanogr. 52, 63–120.

Shenoi, S.S.C., Saji, P.K., Almeida, A.M., 1999. Near-surface circulation and kinetic energy in the tropical Indian Ocean derived from Lagrangian drifters. J. Mar. Res. 57, 885–907.

Shetye, S.R., Gouveia, A.D., Shankar, D., Shenoi, S.S.C., Vinayachandran, P.N., Sundar, D., Michael, G.S., Nampoothiri, G., 1996. Hydrography and circulation in the western Bay of Bengal during the northeast monsoon. J. Geophys. Res. – Oceans 101 (C6), 14011–14025.

Tang, W., Fore, A., Yueh, S., Lee, T., Hayashi, A., Sanchez-Franks, A., et al., 2017. Validating SMAP SSS with in situ measurements. Remote Sens. Environ. 200, 326–340. https://doi.org/10.1016/j.rse.2017.08.021.

Vinayachandran, P.N., Shankar, D., Vernekar, S., Sandeep, K.K., Amol, Neema, C.P., Chatterjee, A., 2013. A summer monsoon pump to keep the Bay of Bengal salty. Geophys. Res. Lett. 40, 1777–1782. https://doi.org/10.1002/grl.50274.

Vinayachandran, P.N., Masumoto, Y., Mikawa, T., Yamagata, T., 1999. Intrusion of the southwest monsoon current into the Bay of Bengal. J. Geophys. Res. – Oceans 104 (C5), 11077–11085.

Vinayachandran, P.N., Yamagata, T., 1998. Monsoon response of the sea around Sri Lanka: generation of thermal domes and anticyclonic vortices. J. Phys. Oceanogr. 28, 1946–1960.

Webber, B.G.M., Matthews, A.J., Vinayachandran, P.N., Neema, C.P., Sanchez-Franks, A., Vijith, V., Amol, P., Barabowski, D.B., 2018. The dynamics of the Southwest Monsoon Current in 2016 from high-resolution in situ observations and models. J. Phys. Oceanogr. 48, 2259–2282. https://doi.org/10.1175/JPO-D-17-0215.1.

Wijesekera, H.W., Jensen, T.G., Jarosz, E., Teague, W.J., Metzger, E.J., Wang, D.W., Jinadasa, S.U.P., Arulananthan, K., Centurioni, L.R., Fernando, H.J.S., 2015. Southern Bay of Bengal currents and salinity intrusions during the northeast monsoon. J. Geophys. Res. – Oceans 120, 6897–6913. https://doi.org/10.1002/2015JC010744.

Wijesekera, H.W., Shroyer, E., Tandon, A., Ravichandran, M., Sengupta, D., Jinadasa, S.U.P., et al., 2016. ASIRI: an ocean-atmosphere initiative for Bay of Bengal. Bull. Am. Meteorol. Soc. 97 (10), 1859–1884. https://doi.org/10.1175/BAMS-D-14-00197.1.

Wyrtki, K., 1973. An equatorial jet in the Indian Ocean. Science 181, 262–264.